Trends in adsorption of noble gases He, Ne, Ar, Kr, and Xe on Pd(111)($\sqrt{3}\times\sqrt{3}$)*R*30°: All-electron density-functional calculations

Juarez L. F. Da Silva[1,*] and Catherine Stampfl[2,†]
[1]*Fritz-Haber-Institut der Max-Planck-Gesellschaft, Faradayweg 4-6, D-14195 Berlin, Germany*
[2]*The School of Physics, The University of Sydney, Sydney, New South Wales 2006, Australia*
(Received 5 May 2007; revised manuscript received 4 September 2007; published 2 January 2008)

It was recently found from *ab initio* investigations [J. L. F. Da Silva *et al.*, Phys. Rev. Lett. **90**, 066104 (2003)] that polarization effects and the site dependence of the Pauli repulsion largely dictate the nature of the interaction and the site preference of Xe adatoms on close-packed metal surfaces. It is unclear if the same interaction mechanism occurs for *all* rare-gas atoms adsorbed on such surfaces. To address this question, we perform all-electron density-functional theory calculations with the local-density approximation (LDA) and generalized gradient approximations (GGA) for [He, Ne, Ar, Kr, and Xe]/Pd(111) in the ($\sqrt{3}\times\sqrt{3}$)*R*30° structure. Our results confirm that polarization effects of the rare-gas adatoms and Pd atoms in the topmost surface layer, together with the site-dependent Pauli repulsion, largely determine the interaction between rare-gas atoms and the Pd(111) surface. Similar to the earlier *ab initio* study, the on-top site preference is obtained by the LDA for all rare-gas adatoms, while the GGA functionals yield the on-top site preference for Xe, Kr, and He adatoms, but the fcc site for Ne and Ar.

DOI: 10.1103/PhysRevB.77.045401 PACS number(s): 68.43.Bc, 68.43.Fg, 68.43.Mn, 71.15.Mb

I. INTRODUCTION

The adsorption of rare-gas (RG) atoms on solid surfaces is a classical example of physical adsorption systems,[1] in which the binding energy ranges from a few meV to a few hundred meV, e.g., −10 meV for He/Pd(110), −24 meV for Ne/Pd(110), −200 meV for Kr/Pd(100), and −320 to −360 meV for Xe/Pd(111).[2–5] Rare-gas atoms have long been used in different experimental techniques to probe solid surfaces. For example, atom scattering using He and Ne atoms,[6] nuclear magnetic resonance using ^{129}Xe atoms,[7,8] photoemission of adsorbed Xe atoms,[9] and high energy Ar ions have been used for many years to clean solid surfaces and to measure local electrostatic fields. Rare-gas atoms have also been used to create local strain at solid surfaces by formation of subsurface Ar, Kr, and Xe bubbles.[10–13] Furthermore, the adsorption of RG atoms on solid surfaces has a long tradition in serving as a model system to obtain an understanding at the atomic level of technological process, e.g., friction and tribological issues.[14] Thus, a microscopic understanding of the interaction between RG atoms and solid surfaces is important for a correct interpretation of experimental results, but it is also important for advancing fundamental knowledge on adsorption processes. As we will show below, recent studies have obtained an improved understanding of the interaction between Xe atoms and metal surfaces; however, it is unclear if the same picture can be generalized for Kr, Ar, Ne, and He atoms adsorbed on metal surfaces.

Recent low-energy electron diffraction (LEED) intensity analyses of Xe adatoms on Ru(0001),[15,16] Cu(111),[17,18] Pt(111),[18,19] Pd(111),[18,20] and Cu(110) (Refs. 18 and 21), and density-functional theory (DFT) calculations for Xe on Pt(111),[22–26] Pd(111),[24–26] Cu(111),[24–27] Ag(001),[28] Ti(0001),[24–26] Mg(0001),[24–26] and Al(111) (Refs. 24–26) have found that the adsorbates preferentially bind to the low-coordinated on-top sites instead of the high-coordinated hollow sites on metal surfaces. These findings were somewhat unexpected as the long held view was that RG atoms would adsorb in the highly coordinated hollow site (see e.g., Ref. 18 for a recent review). However, LEED[29] and DFT[30,31] studies have found that Xe atoms adsorb preferentially in the hollow site on the graphite (0001) surface. Therefore, the Xe on-top site preference appears to be an updated "general rule" only on metal surfaces.

In earlier publications,[24–26] we explained the on-top Xe adsorption site preference on metal surfaces as being due to the following findings: (i) The polarization is larger for Xe in the on-top site, i.e., the induced dipole moment is greater, which contributes a greater attractive interaction between Xe and the metal surfaces. (ii) The Pauli repulsion is weaker for Xe adatoms at the on-top site, giving rise to a smaller contribution to the repulsive potential between Xe and the metal surfaces, i.e., enhancing the on-top site preference. This behavior was explained on the basis of the reactivity of the clean metal surfaces, such as Pd(111), Pt(111), Cu(111), and Ti(0001).[24] Analyzing the reactivity function of the clean surfaces using the "Wilke function"[32] shows that the electronic character at the on-top region is donorlike and in the hollow site it is acceptorlike. Thus, for a negative charge not too close to the surface (or for a dipole moment with the negative end pointing toward the metal surface like for the RG adsorbate), the on-top site region can easily screen this perturbation by transferring electron density from the on-top region to the hollow site region. Therefore, at intermediate distances, the Xe atom becomes polarized more strongly at the on-top geometry, because the screening charge at the metal surface can build up more efficiently. This is why the induced dipole moment is greater for Xe in the on-top site. Similarly, at close distances where wave functions start to overlap and Pauli repulsion sets in, the substrate can reduce this repulsion more efficiently at the on-top site by transferring electrons from the on-top site region to the hollow site region; hence, Xe can get closer to the surface at the on-top site.

Recent LEED studies obtained evidence for the on-top site preference also for Kr/Ru(0001),[15,16] Kr/Cu(110),[18,33] and Ar/Ag(111).[18,34] Furthermore, experimental studies[4,35,36] have shown a clear decrease in the substrate work function upon adsorption of Kr and Ar atoms. Therefore, these results might indicate a similar interaction mechanism for Kr and Ar adatoms on metal surfaces. However, this assumption is unclear due to the small electronic polarizability of the Kr and Ar atoms compared to Xe atoms, which may decrease the role of the polarization effects in the interaction mechanism. The electronic polarizabilities of the RG atoms are 0.201×10^{-24}, 0.390×10^{-24}, 1.62×10^{-24}, 2.46×10^{-24}, and 3.99×10^{-24} cm^3 for He, Ne, Ar, Kr, and Xe atoms, respectively.[37]

Therefore, it is interesting and important to learn if the model proposed in Refs. 24–26 for Xe adsorption on metal surfaces holds for other RG atoms such as He, Ne, Ar, and Kr. To address this question, we investigate, using all-electron DFT calculations, the trends in the adsorption energy, adsorption site preference, equilibrium structural parameters, work function changes (induced dipole moment), electron density changes, and electronic structure (density of states) for He, Ne, Ar, Kr, and Xe adsorbed on Pd(111) in the $(\sqrt{3}\times\sqrt{3})R30°$ structure (hereafter denoted as "$\sqrt{3}$").

The paper is organized as follows. In Sec. II, the theoretical approach and computational details are described, and in Sec. III, results for He, Ne, Ar, Kr, and Xe adatoms on Pd(111) are presented and discussed. In Sec. IV, the role of electronic polarizability of the free RG atoms in the adsorption properties is discussed, and in Sec. V, the mechanism for the interaction between RG atoms and metal surfaces is described. Section VI presents a discussion of the behavior of the different exchange-correlation functionals, and the main conclusions are given in Sec. VII.

II. THEORETICAL APPROACH AND COMPUTATIONAL DETAILS

A key problem when studying RG adsorption on solid surfaces by DFT[38,39] is the choice of the exchange-correlation (XC) functional. All-electron first-principles calculations[40] found that the generalized gradient approximation (GGA), namely, the GGA-PW91 functional,[41] yields a superior description of the interaction between He and Ne adatoms with Rh(110) compared to the local-density approximation (LDA).[42] For example, GGA-PW91 reproduces the experimental surface corrugation, as well as the potential well if the zero-point vibration is included, while LDA yielded quantities in poor agreement with experimental results.[40] In contrast, recent all-electron calculations found an opposite behavior for Xe adsorption on metal surfaces,[24–26] for which the LDA yielded a better description than the GGA-PBE functional,[43] e.g., the LDA adsorption energies are in good agreement with experimental results, while the GGA-PBE yielded much too weak adsorption energies. It is well known that the GGA-PBE and GGA-PW91 functionals yield almost identical binding properties for many systems;[43] however, recent studies have found important differences in the binding energy E_b of RG molecular systems calculated using these two particular GGA functionals, e.g., E_b=6.1 meV (GGA-PBE) and 14.2 meV (GGA-PW91) for Ar_2,[44] which suggest that possibly the tiny differences between GGA-PBE and GGA-PW91 may play an important role in the interaction between RG atoms and metal surfaces as well. Therefore, in order to obtain a more complete picture for the interaction between RG atoms with metal surfaces, we performed DFT calculations with the LDA,[42] GGA-PBE,[43] and GGA-PW91 functionals.[41]

The Kohn-Sham equations are solved using the all-electron full-potential linearized augmented plane-wave (FP-LAPW) method,[45] as implemented in the WIEN code,[46] which is one of the most accurate methods currently used to solve the Kohn-Sham equations. Furthermore, the FP-LAPW method is commonly used as a reference for benchmark calculations in the study of the performance of XC functionals for periodic systems,[47–49] as well as a reference for pseudopotential calculations.[49] In the FP-LAPW method, real space is divided into two regions, namely, nonoverlapping atom centered spheres and the remaining interstitial region. This definition is only used to define the augmentation for the plane waves and does not imply a shape restriction of the potential or the electron density. The core states are treated fully relativistically, while the semicore and valence states are treated by the scalar relativistic approximation.

The LAPW wave functions in the interstitial region are represented using a plane-wave expansion, truncated to include only plane waves that have kinetic energies less than 14.06 Ry, and for the potential representation in the interstitial region, plane waves with energies up to 196 Ry (LDA) and 324 Ry (GGA-PBE and GGA-PW91) are considered. Inside the atom centered spheres with radii of 0.95, 1.06, 1.16, 1.27, 1.38, and 1.27 Å for He, Ne, Ar, Kr, Xe, and Pd, respectively, the wave functions are expanded in radial functions times spherical harmonics up to $l_{max}^{wf}=12$. For the representation of the potential inside the muffin-tin spheres, a maximum of $l_{max}^{pot}=6$ is used. For the evaluation of the nonspherical matrix elements, we include terms up to $l_{max}^{ns}=6$. The linearization energies are set to be at the center of gravity of the occupied band with the respective character (s,p,d,f). Local orbitals (LOs) are used to describe the semicore states. Furthermore, extra LOs are added to improve the description of the valence Pd d states.

The Pd(111) surface is modeled by a repeated slab, which consists of seven atomic layers separated by a vacuum region of ≈27.50 Å. For the integrations of the Brillouin zone (BZ) of RG/Pd(111) in the $\sqrt{3}$ structure, we employ a Monkhorst-Pack[50] $(8\times8\times1)$ grid (21 **k** points in the irreducible part of the BZ) with the broadening of the Fermi surface by the Fermi distribution function with an artificial broadening parameter of 54 meV. The total energy is extrapolated to $T=0$ K.[51] Exactly the same **k** point set is used for all RG/Pd(111) calculations to minimize possible errors in the BZ integration.

For all RG/Pd(111) calculations, we used the theoretical equilibrium lattice constant a_0 of bulk Pd, which is critical for obtaining an accurate description of the surface properties.[24,52] We found a_0=3.85 Å (LDA), 3.95 Å (GGA-PBE), 3.95 Å (GGA-PW91), as obtained by fitting to Murnaghan's equation of state,[53] while the experimental lattice

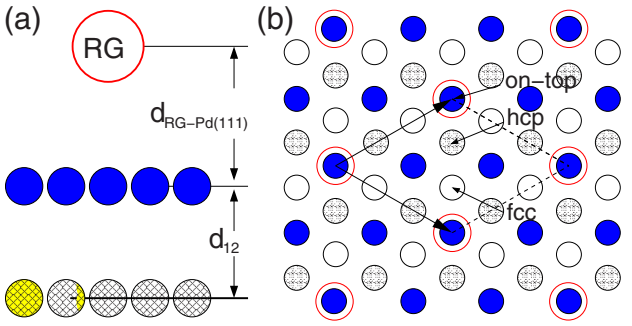

FIG. 1. (Color online) (a) Illustration showing the equilibrium vertical distance between the RG adatom and the Pd(111) surface, $d_{\text{RG-Pd(111)}}$, and the topmost interlayer distance, d_{12}. (b) Adsorption sites for RG adatoms on Pd(111) in the $\sqrt{3}$ structure. The indicated adsorption sites are: on-top, fcc, and hcp sites. For (a) and (b), the RG adatoms are indicated by large open circles (red), while the filled, hatched, and open small circles (in blue, yellow, and white, respectively) indicate the Pd atoms in the first (topmost surface layer), second, and third substrate layers, respectively.

constant is 3.89 Å.[37] A more detailed discussion of the Pd bulk properties is given elsewhere.[24,52]

In this work, we deal with the weak interaction of RG atoms with the Pd(111) surface, where the relative energy differences, work function changes, etc., are very small. For example, the energy difference between the on-top and fcc sites is 44.1meV (LDA) for Xe/Pd(111); hence, special care was taken with respect to the numerical parameters involved in the calculations. Calculations using a higher cutoff energy (18.65 Ry) for Xe/Pd(111) yielded equilibrium vertical distances, relative energy difference between the on-top and fcc sites, and work function changes that differ by less than 0.05 Å, 1.0 meV, and 0.02 eV, respectively, compared with the results calculated with 14.06 Ry. Furthermore, calculations using a higher number of **k** points, e.g., 31 **k** points in the IBZ, yielded almost identical equilibrium vertical distances, while the relative energy difference for Xe adatoms in the on-top and fcc sites and work function changes differ by less than 1.5 meV and 0.01 eV, respectively, compared with calculations using 21 **k** points in the IBZ.

III. RARE-GAS ADATOMS ON Pd(111) IN THE $\sqrt{3}$ STRUCTURE

All calculations for the adsorption of RG adatoms on Pd(111) are performed using the $\sqrt{3}$ structure, in which the RG coverage Θ_{RG} is $\frac{1}{3}$, i.e., one RG adatom for each three metal atoms in the topmost surface layer [see Fig. 1(b)]. The $\sqrt{3}$ structure has been reported by LEED studies for Xe adsorption on several close-packed transition-metal surfaces, namely, Pd(111),[2,5,20] Cu(111),[17,36] Pt(111),[19,54,55] and Ru(0001).[15] The $\sqrt{3}$ structure is a simple structure compared to other commensurate[21] and incommensurate[54] structures reported for Xe adsorption. For example, a (12×2) structure has been obtained by LEED for Xe/Cu(110), for which $\Theta_{\text{Xe}}=\frac{7}{12}$.[21] For Kr and Ar, LEED studies have reported large unit cell structures, e.g., $c(8\times2)$ for Kr/Cu(110) with $\Theta_{\text{Kr}}=\frac{5}{8}$,[33] $p(3\times3)$ for Kr/Ru(0001) with $\Theta_{\text{Kr}}=\frac{6}{9}$,[15,16] and $(\sqrt{7}\times\sqrt{7})R19.1°$ for Ar/Ag(111) with $\Theta_{\text{Ar}}=\frac{4}{7}$.[34] Due to the lower temperatures required for the study of Ne and He adlayers on metal surfaces, there are no reports of LEED studies for these systems.

All-electron calculations performed for Xe/Ag(100) (Ref. 28) and Xe/Pt(111) (Refs. 24–26) found that spin-orbit (SO) coupling, which can be included for the semicore and valence states using the second-variational method,[45] does not play a significant role in adsorption properties such as adsorption energy, site preference, work function change, electron density difference, etc. However, the SO interaction is required to obtain the correct band structure of the Xe adlayer, i.e., it reproduces the splitting of the Xe $5p$ states into $5p_{1/2}$ and $5p_{3/2}$ states. As we are only concerned with total energies, forces, and geometries in this paper, SO corrections for the semicore and valence states are not taken into account.

In our previous DFT studies,[24–26] we found that the on-top and fcc sites are the most, and the least, stable adsorption sites for Xe adatoms on closed-packed transition-metal surfaces, respectively. Thus, in the present work, we performed calculations for RG adatoms only in the on-top and fcc sites [see Fig. 1(b)]. Furthermore, we found that the interlayer relaxations of the topmost surface layers for the Xe/metal systems, as well as the substrate rumpling for Xe adatoms in the on-top sites, do not play a significant role in the interaction mechanism between Xe adatoms and metal surfaces. For Pd(111), the topmost interlayer spacing exhibits a very small relaxation ($\Delta d_{12}<1.50\%$).[24,52] Thus, for all calculations reported below, the Pd atoms are kept frozen in their truncated bulk positions and only the coordinates of the RG atoms perpendicular to the surface are optimized.

A. Adsorption energy

The adsorption energy $E_{\text{ad}}^{\text{RG}}$ of a RG adatom on Pd(111) is given by

$$E_{\text{ad}}^{\text{RG}}=\frac{1}{2}(E_{\text{tot}}^{\text{RG/Pd(111)}}-E_{\text{tot}}^{\text{Pd(111)}}-2E_{\text{tot}}^{\text{RG}}), \tag{1}$$

where $E_{\text{tot}}^{\text{RG/Pd(111)}}$ is the total energy of the RG/Pd(111) system at the equilibrium geometry. $E_{\text{tot}}^{\text{Pd(111)}}$ and $E_{\text{tot}}^{\text{RG}}$ are the total energies of the clean Pd(111) surface and of the free RG atoms, respectively. The factors $\frac{1}{2}$ and 2 take into account the fact that the RG atoms are adsorbed on both sides of the slab. The total energies of the free RG atoms are obtained by spin-polarized calculations using a cubic box with side length of 9.52 Å and one **k** point, $(\frac{1}{4},\frac{1}{4},\frac{1}{4})\frac{2\pi}{a}$, in the irreducible part of the BZ.[49] The calculated adsorption energies are summarized in Table I along with experimental results. For He, Ne, Ar, and Kr adatoms on Pd(111), the reported experimental values are estimated based on experimental results for Pd(100) and Pd(110) (see discussion below).[3–5,56]

The LDA and GGA-PW91 adsorption energies increase from He to Xe; however, the increase is much smaller for the GGA-PW91 functional than for the LDA functional. This can be clearly seen from Fig. 2. For example, the LDA ad-

TABLE I. Adsorption energy E_{ad}^{RG} (in meV) of RG adatoms on Pd(111) in the on-top site for the $\sqrt{3}$ structure.

XC	He	Ne	Ar	Kr	Xe
LDA	−26.7	−63.9	−159.3	−225.4	−435.4
GGA-PBE	−5.0	−13.5	−14.9	−14.3	−55.3
GGA-PW91	−16.3	−28.4	−33.3	−50.4	−79.3
Expt.[a]	−8	−19	−110	−177	−320, −360

[a]Experimental results (estimated for He, Ne, Ar, and Kr, see text), Refs. 3–5 and 56.

sorption energy ratios E_{ad}^{Xe}/E_{ad}^{RG} are 1.93 (Kr), 2.73 (Ar), 6.82 (Ne), and 16.32 (He), while the GGA-PW91 correspondingly yields 1.57 (Kr), 2.38 (Ar), 2.79 (Ne), and 4.85 (He). Using the LDA ratio for E_{ad}^{Xe}/E_{ad}^{He}, i.e., 16.32, and the GGA-PW91 adsorption energy obtained for Xe (−79.27), we estimate an adsorption energy of −4.86 meV for He, which is close to the GGA-PBE value but far from the GGA-PW91 value (−16.34 meV). We found that the GGA-PBE yields almost the same adsorption energy (≈14 meV) for Ne, Ar, and Kr, which is different from the LDA and GGA-PW91 trends (see Fig. 2, Table I). The GGA-PBE result for E_{ad}^{Xe}/E_{ad}^{He} is 11.08, which is in between the LDA and GGA-PW91 results.

We note that a similar trend has been reported for the binding energies E_b of RG diatomic molecules.[44] For example, employing GGA-PBE, E_b=3.2 meV for He_2 and ≈6 meV for Ne_2, Ar_2, and Kr_2, while the LDA binding energies increase systematically with the atomic number, i.e., 9.4, 19.9, 28.9, and 33.5 meV for He_2, Ne_2, Ar_2, and Kr_2, respectively.[44] For comparison, the exact values[57,58] are 0.9, 3.6, 12.3, and 17.3 meV for He_2, Ne_2, Ar_2, and Kr_2, respectively, which are larger (smaller) than the GGA-PBE (LDA) values but display a clear trend of increasing binding energy with increasing size of the RG atom.

There are available experimental adsorption energies only for the particular case of Xe/Pd(111), namely, −338 and −320±10 meV for Xe in the $\sqrt{3}$ structure,[2,5] while it is

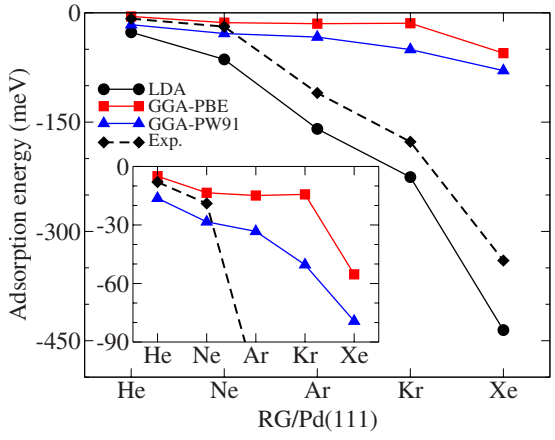

FIG. 2. (Color online) Adsorption energy of RG adatoms on Pd(111) in the $\sqrt{3}$ structure in the on-top site. An inset is included to show in detail the GGA (PBE and PW91) results. The black dashed line (diamond symbol) indicates estimated experimental results (see text for details) (Refs. 3–5 and 56).

−360 meV for the limit of zero Xe coverage.[2] For the other RG adatoms, there are reported adsorption energies only for Pd(110) and Pd(100), i.e., −10 meV for He/Pd(110), −24 meV for Ne/Pd(110), and −200 meV for Kr/Pd(100).[3,4] In this work, we estimate the experimental adsorption energies of He, Ne, Ar, and Kr adatoms on Pd(111) using the results above and the adsorption energy ratios for Xe on Pd(111), Pd(100), and Pd(110). For example, E_{ad}^{Xe}=−338, −381, and −425 meV for (111), (100), and (110), respectively, and hence, we obtain $\frac{E_{ad}^{Xe}(100)}{E_{ad}^{Xe}(111)}$=1.127 and $\frac{E_{ad}^{Xe}(110)}{E_{ad}^{Xe}(111)}$=1.257.[56] Thus, we estimate E_{ad}^{RG} as −8, −19, −110, and −177 meV for He, Ne, Ar, and Kr adatoms on Pd(111). To estimate E_{ad}^{Ar}, we used the relation $\frac{E_{ad}^{Xe}}{E_{ad}^{Ar}}\approx 3$, which is obtained from the experimental adsorption energies reported in Ref. 4. The estimated experimental adsorption energies are show in Fig. 2 (dashed line) along with the calculated results.

It can be seen from Fig. 2 that the LDA adsorption energies are in much closer agreement with the experimental results for Ar, Kr, and Xe than the GGA functionals, while the results for He and Ne adatoms are overestimated. The GGAs (PBE and PW91) underestimate the adsorption energies for Ar, Kr, and Xe adatoms, while GGA-PBE (GGA-PW91) underestimates (overestimates) for He and Ne. It is important to notice that LDA yields the correct trend, and the shape of the curve appears very close to experiment, but just shifted uniformly to lower energies, which is not the case of the GGA functionals, in particular the GGA-PBE. For example, from the experimental adsorption energies summarized in Ref. 4, we find that $\frac{E_{ad}^{Xe}}{E_{ad}^{Kr}}\approx 2$ and $\frac{E_{ad}^{Xe}}{E_{ad}^{Ar}}\approx 3$ for several close-packed transition-metal surfaces. This is in good agreement with the LDA adsorption energy ratios discussed above (i.e., 1.93 and 2.73), but not so for the GGA adsorption energy ratios (of 3.86 and 3.71 for the PBE and 1.57 and 2.38 for the PW91).

The relative adsorption energies of RG adatoms in the fcc and on-top sites, $\Delta E_{ad}^{RG}=E_{ad}^{RG}(\text{fcc})-E_{ad}^{RG}(\text{on-top})$, are given in Table II. $\Delta E_{ad}^{RG}>0$ (<0) indicates an on-top (fcc) adsorption site preference. The LDA functional favors the on-top site for all RG adatoms on Pd(111), which is consistent with LEED studies of RG atoms adsorbed on different metal surfaces, e.g., Ar/Ag(111),[34] Xe/Ru(0001),[15,16] Kr/Ru(0001),[15,16] Xe/Cu(111),[17] Xe/Pd(111),[20] Kr/Cu(110),[33] and Xe/Cu(110).[21] The GGA-PW91 and GGA-PBE functionals, however, yield the on-top site preference only for Xe, Kr, and He adatoms, while Ne and Ar preferentially bind to the fcc sites. We note that for both GGA functionals, ΔE_{ad}^{RG} is smaller than 1 meV for Ne/Pd(111); hence, this result

TABLE II. Relative adsorption energies ΔE_{ad}^{RG} (in meV) of RG adatoms in the fcc and on-top sites on Pd(111) in the $\sqrt{3}$ structure. $\Delta E_{ad}^{RG} > 0 (< 0)$ indicates an on-top (fcc) adsorption site preference.

XC	He	Ne	Ar	Kr	Xe
LDA	+4.0	+1.9	+18.0	+13.9	+44.1
GGA-PBE	+2.5	−0.7	−4.0	+7.8	+6.3
GGA-PW91	+1.4	−0.7	−4.4	+7.4	+10.0

should not be taken too seriously since it is at the limit of our accuracy, even though the FP-LAPW calculations have been carried out at a high level of accuracy (see Sec. II).

B. Equilibrium rare-gas–Pd(111) distances

The equilibrium distances between the RG adlayers and the Pd(111) surface, $d_{\text{RG-Pd(111)}}$, which is defined in Fig. 1, are listed in Table III. We find using the LDA, GGA-PBE, and GGA-PW91 functionals that the Ar, Kr, and Xe adatoms get closer to the Pd(111) surface in the on-top sites, i.e.,

$$d^{\text{on-top}}_{\text{[Ar,Kr,Xe]-Pd(111)}} < d^{\text{fcc}}_{\text{[Ar,Kr,Xe]-Pd(111)}}. \quad (2)$$

This trend was also found from FP-LAPW calculations for Xe atoms adsorbed on the Mg(0001), Al(111), Ti(0001), Cu(111), Pd(111), and Pt(111) surfaces.[24–26] In Refs. 24–26, from a decomposition of the perpendicular potential energy surface into an attractive and repulsive potential term, the smaller equilibrium distance for Xe adatoms in the on-top sites was explained as a consequence of a weaker Pauli repulsion for Xe adatoms in the on-top sites. This weaker repulsion at the on-top site was attributed to a greater polarization of the Xe atoms and the substrate atoms, which decreases the electron density at the on-top site and allows the Xe atoms to get closer to the surface. This explanation is supported by our electron density redistribution analysis below.

For Ne/Pd(111), we find using the LDA functional that $d^{\text{on-top}}_{\text{Ne-Pd(111)}} > d^{\text{fcc}}_{\text{Ne-Pd(111)}}$, while both GGA (PBE and PW91) calculations find that $d^{\text{on-top}}_{\text{Ne-Pd(111)}} \approx d^{\text{fcc}}_{\text{Ne-Pd(111)}}$. For He/Pd(111), the LDA yields $d^{\text{on-top}}_{\text{He-Pd(111)}} < d^{\text{fcc}}_{\text{He-Pd(111)}}$, and hence, it follows the same trend observed for Ar, Kr, and Xe. However, the GGA (PBE and PW91) calculations find an opposite trend, i.e., $d^{\text{on-top}}_{\text{He-Pd(111)}} > d^{\text{fcc}}_{\text{He-Pd(111)}}$. The LDA results for Ne and He may indicate a weaker Pauli repulsion at the fcc and on-top sites, respectively. Thus, this contribution to the adsorption energy decreases (for weaker repulsion at the fcc site) and increases (for weaker repulsion at the on-top site) the stability of the on-top site preference, respectively, which is confirmed by the LDA total energy calculations, i.e., $\Delta E_{ad}^{RG} = 1.9$ and 4.0 meV for Ne and He adatoms on Pd(111). The GGA (PBE and PW91) results for Ne indicate a similar repulsive potential for both sites, which is consistent with the GGA total energy calculations, i.e., both sites are almost degenerate in energy ($|\Delta E_{ad}^{RG}| < 1.0$ meV). Therefore, the trends found for He and Ne are slightly different to the results found for Ar, Kr, and Xe, which may be related to the notably smaller electronic polarizability of the free He and Ne atoms as compared to the Ar, Kr, and Xe atoms, and hence, it implies a small polarization of the He and Ne adatoms and of the topmost surface Pd atoms.

For all functionals, the equilibrium vertical distance *increases* from Xe to Ar; hence, it correlates with the magnitude of the adsorption energy, which decreases in absolute value from Xe to Ar (i.e., a larger adsorbate-substrate bond and a weaker adsorption energy). However, the results obtained for Ne and He do not follow the same trend for all functionals and adsorption sites. To obtain a further understanding of the equilibrium distance trends, we calculated the expected equilibrium distances using a hard-sphere model for RG adatoms on Pd(111). Using experimental lattice constants,[37] we obtain equilibrium distances of 3.55, 3.38, 3.26, 2.96, and 3.17 Å for Xe, Kr, Ar, Ne, and He adatoms on Pd(111) in the on-top site, respectively. The trend in these results obtained for Xe, Kr, and Ar are *opposite* to the trends

TABLE III. Equilibrium distances $d_{\text{RG-Pd(111)}}$ of RG adatoms on Pd(111) in the $\sqrt{3}$ structure. $d_{\text{RG-Pd(111)}}$ is given in Å with respect to the topmost surface layer.

	Site	He	Ne	Ar	Kr	Xe
LDA	on-top	2.887	2.898	2.956	2.938	2.835
	fcc	3.008	2.885	2.994	2.970	2.859
GGA-PBE	on-top	3.649	3.408	3.578	3.543	3.294
	fcc	3.416	3.408	3.761	3.655	3.489
GGA-PW91	on-top	3.644	3.404	3.561	3.481	3.278
	fcc	3.405	3.394	3.752	3.648	3.479
Expt.						3.07[a]

[a]Ref. 20, LEED.

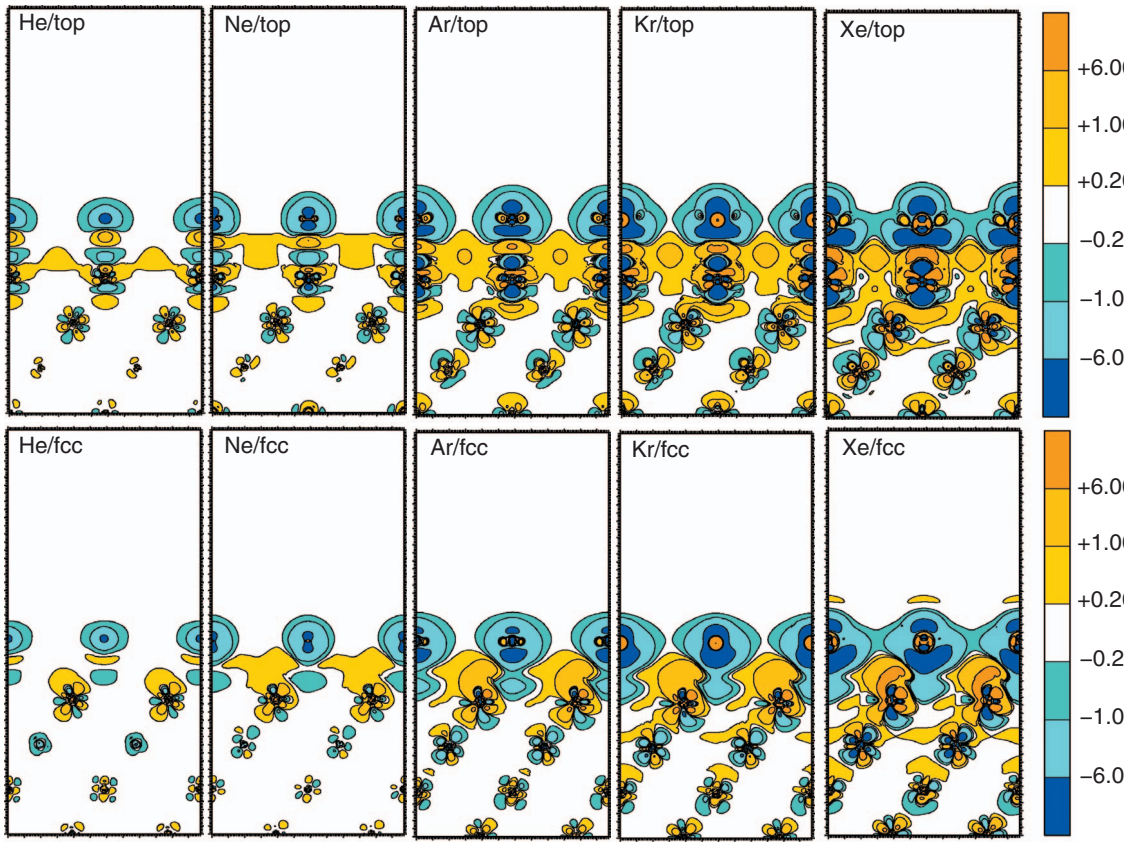

FIG. 3. (Color) Difference electron density, $n^{\Delta}(\mathbf{r})=n^{\mathrm{RG/Pd(111)}}(\mathbf{r})-n^{\mathrm{Pd(111)}}(\mathbf{r})-n^{\mathrm{RG\text{-}layer}}(\mathbf{r})$, distributions calculated using the LDA for He, Ne, Ar, Kr, and Xe (from left to right) adatoms on the Pd(111) surface in the $\sqrt{3}$ structure for RG adatoms in the on-top (upper) and fcc (lower) sites. $n^{\Delta}(\mathbf{r})$ is in units of 10^{-3} e/bohr^3 and plotted in the $(11\bar{2})$ plane at the equilibrium geometry. Yellow, gold, and orange (cyan, sky blue, and blue) indicate regions where the electron density increases (decreases).

actually calculated by LDA, GGA-PBE, and GGA-PW91 (see Table II) showing that there is a significant interaction between the Xe, Kr, and Ar atoms and the Pd(111) surface and that a simple stacking (hard sphere) model of weakly or noninteracting spheres is not valid. However, the hard-sphere model yields that $d_{\mathrm{He\text{-}Pd(111)}}>d_{\mathrm{Ne\text{-}Pd(111)}}$, which is consistent with the LDA, GGA-PBE, and GGA-PW91 results. The success of the hard-sphere model in predicting results for [He,Ne]/Pd(111) can be explained as a consequence of the small electronic polarizability of He and Ne atoms.

For Xe/Pd(111), the LDA and GGA equilibrium lattice constants are 7.6% and 7.3% smaller and larger, respectively, than the LEED result of 3.07 Å. LEED studies for Xe and Kr adsorption on Ru(0001) reported equilibrium distances of 3.54 and 3.70 Å, respectively, i.e., $d_{\mathrm{Kr\text{-}Ru(0001)}}$ is 4.5% larger than $d_{\mathrm{Xe\text{-}Ru(0001)}}$. We find using the LDA and GGA that $d_{\mathrm{Kr\text{-}Pd(111)}}$ is 3.6% and 7.6% larger than $d_{\mathrm{Xe\text{-}Pd(111)}}$, respectively. Thus, the qualitative trends are well reproduced regarding the Xe– and Kr–transition-metal distances.

C. Difference electron density

The difference electron density, which helps characterize the atomic orbitals involved in the interaction between two different systems, is given by

$$n^{\Delta}(\mathbf{r})=n_{\mathrm{tot}}^{\mathrm{RG/Pd(111)}}(\mathbf{r})-n_{\mathrm{tot}}^{\mathrm{Pd(111)}}(\mathbf{r})-n_{\mathrm{tot}}^{\mathrm{RG\text{-}layer}}(\mathbf{r}), \quad (3)$$

where $n_{\mathrm{tot}}^{\mathrm{RG/Pd(111)}}(\mathbf{r})$ is the total electron density of the RG/Pd(111) system. $n_{\mathrm{tot}}^{\mathrm{Pd(111)}}(\mathbf{r})$ and $n_{\mathrm{tot}}^{\mathrm{RG\text{-}layer}}(\mathbf{r})$ are the total electron densities of the Pd(111) surface and the RG layer, respectively. We calculate $n^{\Delta}(\mathbf{r})$ for the RG/Pd(111) systems at the equilibrium geometry in a plane perpendicular to the surface, i.e., $(11\bar{2})$. The results obtained with the LDA functional are shown in Fig. 3. It can be seen that the difference electron densities for Ar, Kr, and Xe are very similar. The patterns differ mainly in the magnitude of the induced electron density redistribution, which is smallest for Ar and largest for Xe. The induced electron density redistributions for He and Ne adatoms also show quite similar patterns to the other RG adatoms; however, the magnitude of the electron density redistributions are notably weaker, which is consistent with the smaller electronic polarizabilities of the Ne and He atoms and with the small adsorption energies.

Figure 3 shows that the induced electron density redistribution on the RG adatoms and on the Pd atoms in the topmost surface layer is different for the on-top and fcc sites. In particular, the electron redistribution on the Pd atoms is clearly stronger for the on-top site, where it increases from He to Xe. For the on-top site, there is a decrease of the electron density in the Pd d states perpendicular to the sur-

TABLE IV. Substrate work function change $\Delta\Phi^{RG}$ and induced dipole moment μ^{RG} for the RG/Pd(111) systems in the $\sqrt{3}$ structure in the fcc and on-top sites. $\Delta\Phi^{RG}$ and μ^{RG} are given in eV and Debye, respectively.

		He		Ne		Ar		Kr		Xe	
	Site	$\Delta\Phi$	μ	$\Delta\Phi$	μ	$\Delta\Phi$	μ	$\Delta\Phi$	μ	$\Delta\Phi$	μ
LDA	on-top	−0.167	−0.085	−0.220	−0.112	−0.680	−0.347	−0.963	−0.491	−1.435	−0.732
	fcc	−0.104	−0.053	−0.169	−0.086	−0.541	−0.276	−0.805	−0.410	−1.286	−0.656
GGA-PBE	on-top	−0.027	−0.014	−0.050	−0.027	−0.184	−0.099	−0.322	−0.173	−0.778	−0.418
	fcc	−0.039	−0.021	−0.040	−0.021	−0.105	−0.056	−0.229	−0.123	−0.544	−0.293
GGA-PW91	on-top	−0.014	−0.008	−0.040	−0.022	−0.180	−0.096	−0.358	−0.192	−0.791	−0.424
	fcc	−0.036	−0.019	−0.031	−0.016	−0.098	−0.052	−0.230	−0.123	−0.550	−0.295
Expt.[a]										−0.85	

[a]Experimental result, Ref. 4.

face, i.e., d_{z^2} state, while there is a small increase in the electron density in the "diagonal" d states (d_{xz} and d_{yz} states).

Both sites exhibit a significant depletion of electron density centered about the RG atom, and it can also be noticed that there is a slight electron density accumulation close to the center of the RG adatoms (the small yellow region inside the larger region of depletion). This small enhancement is largest for Xe/Pd(111) with Xe in the on-top site and is attributed to the orthogonalization of RG states to the states of the Pd atoms. Furthermore, for RG adatoms in the on-top site, there is a significant electron density accumulation between the RG adatom and the topmost surface layer, which increases in magnitude from He to Xe.

Although the discussion above is based entirely on the LDA results, similar patterns for the induced electron density difference distributions are found for the GGA-PBE and GGA-PW91 functionals. As reported previously,[24–26] the magnitude of the GGA induced electron density is, however, smaller than the LDA results, which is consistent with the larger equilibrium RG vertical distances yielded by the GGA functionals and the weaker adsorption energies, as well as the smaller changes in the Pd(111) work function (see below).

D. Work function change and induced surface dipole moment

We report the work function change of the RG/Pd(111) systems, $\Delta\Phi^{RG}$, which can be measured experimentally (see, e.g., Refs. 2 and 36), calculated as $\Delta\Phi^{RG}=\Phi^{RG/Pd(111)}-\Phi^{Pd(111)}$, where the first and second terms are the work functions of RG/Pd(111) and the clean Pd(111) surface, respectively. $\Phi^{Pd(111)}=5.66$, 5.25, and 5.31 eV for LDA, GGA-PBE, and GGA-PW91, respectively, while the experimental results are 5.44 eV,[59] 5.55 eV,[60] and 5.95 eV.[2] The experimental and calculated results for $\Phi^{Pd(111)}$ are discussed in detail elsewhere.[52] $\Delta\Phi^{RG}$ can be related to the induced dipole moment μ^{RG} using the Helmholtz equation,[61] which is given by

$$\mu^{RG}(\Theta_{RG}) = \frac{1}{12\pi}\frac{A_{(1\times1)}}{\Theta_{RG}}\Delta\Phi^{RG}(\Theta_{RG}), \tag{4}$$

where $A_{(1\times1)}$ is the area of the (1×1) surface unit cell in Å^2. Θ_{RG} is the RG coverage, i.e., 1/3 for the $\sqrt{3}$ structures. If $\Delta\Phi$ is given in eV, Eq. (4) yields an induced dipole moment in debyes. All results for $\Delta\Phi$ and μ are listed in Table IV, and the results for the dipole moments are also plotted in Fig. 4. $\Delta\Phi$ and μ are related by a constant, i.e., $\sqrt{3}a_0^2/16\pi$; hence, only the induced dipole moment will be discussed below. It can be seen that the RG adsorption induces a decrease in the work function. This indicates that the RG atoms behave as adsorbates with an effective positive charge. This is reflected in the redistribution of electron density by the depletion about the RG atoms giving rise to an induced surface dipole moment which points out of the surface.

The absolute value of the induced surface dipole moment calculated with the LDA, GGA-PBE, and GGA-PW91 functionals increase from He to Xe, i.e., $|\mu^{He}|<|\mu^{Ne}|<|\mu^{Ar}|<|\mu^{Kr}|<|\mu^{Xe}|$ (see Fig. 4). The only exception is for He and Ne adatoms in the fcc site calculated with the GGA-PW91, i.e., $|\mu^{He}|>|\mu^{Ne}|$. Furthermore, we found the following trend for the systems:

$$|\mu^{RG}(\text{on-top})| > |\mu^{RG}(\text{fcc})|, \tag{5}$$

with the exception of He/Pd(111) calculated with the GGA-PBE and GGA-PW91. This trend [Eq. (5)] was found in previous work for Xe adsorption on the Pt(111), Cu(111),

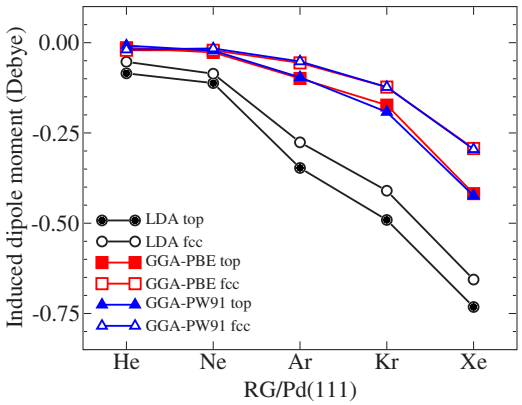

FIG. 4. (Color online) Induced dipole moment of RG adatoms on Pd(111) in the $\sqrt{3}$ structure for adsorption in the on-top (filled symbols) and fcc (open symbols) sites.

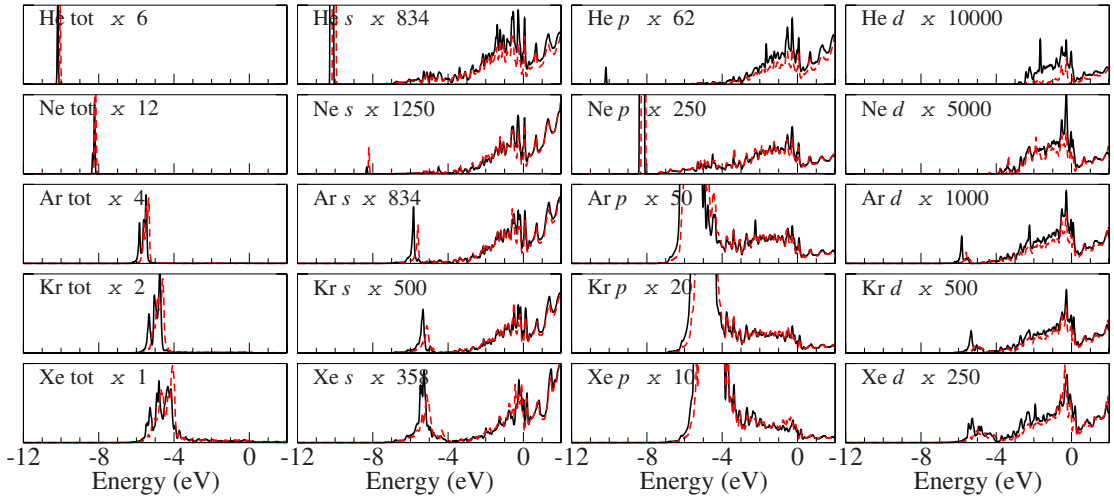

FIG. 5. (Color online) Local density of states (LDOS) calculated with the LDA functional for RG adatoms on Pd(111) in the $\sqrt{3}$ structure at the equilibrium geometry. The continuous and dashed lines in black and red (dark gray) indicate RG adatoms in the on-top and fcc sites, respectively. The zero of energy indicates the Fermi level. The numbers in each plot indicate the factor by which the LDOSs have been multiplied in order to be on the same y scale as the Xe total LDOS. "RG tot" indicates the total LDOS, while s, p, and d indicate the decomposition of the LDOS into states with s, p, and d character.

Ti(0001), Al(111), and Mg(0001) surfaces.[24–26]

For all systems, we find that $|\mu^{\mathrm{RG}}(\mathrm{LDA})| > |\mu^{\mathrm{RG}}(\mathrm{GGA\text{-}PBE/PW91})|$ and $|\mu^{\mathrm{RG}}(\mathrm{GGA\text{-}PBE})| \approx |\mu^{\mathrm{RG}}(\mathrm{GGA\text{-}PW91})|$. At the same equilibrium vertical distance, both LDA and GGA (PW91 and PBE) yield almost the same work function change;[24,26] hence, the difference in the LDA and GGAs work function changes is a consequence of the different equilibrium vertical distances yielded by the LDA and GGA functionals, as well as by the interaction mechanism between RG and metal surfaces. For example, as a consequence of the interaction mechanism, the induced dipole moment and work function change increase almost linearly in absolute values as the RG adatoms approach the Pd(111) surface.[24–26] The linear relationship between $d_{\mathrm{RG\text{-}Pd(111)}}$ and μ^{RG} is valid only for $d_{\mathrm{RG\text{-}Pd(111)}}$ values close to the equilibrium distance between the RG adlayer and Pd(111). For example, the LDA underestimates the value of $d_{\mathrm{RG\text{-}Pd(111)}}$ compared to the GGAs functionals; hence, a larger induced dipole moment is obtained for LDA, while GGA overestimates $d_{\mathrm{RG\text{-}Pd(111)}}$ and has a smaller dipole moment.

E. Local density of states

We calculate the rare-gas local density of states (RG-LDOS), as well as the decomposition of the RG-LDOS into states with s, p, and d character for the RG/Pd(111) systems in the equilibrium geometry for all XC functionals. In addition, we calculated the center of gravity of the RG-LDOS with respect to the Fermi level, $C_{\mathrm{RG}}^{\mathrm{E_F}}$, and vacuum level, $C_{\mathrm{RG}}^{\mathrm{vac}}$. The absolute values of $C_{\mathrm{RG}}^{\mathrm{E_F}}$ and $C_{\mathrm{RG}}^{\mathrm{vac}}$ are related by the work function of the RG/Pd(111) system, i.e., $|C_{\mathrm{RG}}^{\mathrm{vac}}| = |C_{\mathrm{RG}}^{\mathrm{E_F}}| + \Phi^{\mathrm{RG/Pd(111)}}$. The LDA, GGA-PBE, and GGA-PW91 RG-LDOS are very similar; hence, only the LDA results are shown in Fig. 5. The centers of gravity are summarized in Table V for all XC functionals.

As expected from the electronic structure of the free RG atoms, the RG-LDOSs are mainly composed of s states (He) and p states (Ne, Ar, Kr, and Xe), which are shifted several electron volts below the vacuum level on adsorption. We found that $C_{\mathrm{RG}}^{\mathrm{vac}}$ increases in absolute value from Xe to He, e.g., $|C_{\mathrm{RG}}^{\mathrm{vac}}|(\mathrm{LDA}) = 8.57$ eV (Xe) and 15.62 eV (He) for adsorption in the on-top sites. To understand the magnitude of the RG-LDOS shifts, we calculated the energy of the highest occupied state of the free RG atoms with respect to the vacuum level, $\varepsilon_{\mathrm{RG}}$. The results are also summarized in Table V. We find a clear correlation between $C_{\mathrm{RG}}^{\mathrm{vac}}$ and $\varepsilon_{\mathrm{RG}}$ for all RG adatoms, and it does not depend on the adsorption site preference or XC functional, i.e., $C_{\mathrm{RG}}^{\mathrm{vac}}$ and $\varepsilon_{\mathrm{RG}}$ differ only slightly. For example, for Xe $|C_{\mathrm{Xe}}^{\mathrm{vac}} - \varepsilon_{\mathrm{Xe}}| \approx 0.20$ eV and for He $C_{\mathrm{He}}^{\mathrm{vac}} \approx \varepsilon_{\mathrm{He}}$. The difference is larger for the more strongly interacting system, i.e., Xe/Pd(111). Therefore, the magnitude of $C_{\mathrm{RG}}^{\mathrm{vac}}$ for RG adatoms on Pd(111) is determined by the energy of the highest occupied state of the free RG atoms and not by the substrate. This can be explained as a simple consequence of the weak interaction between RG atoms and Pd(111), which does not change very much the center of gravity of the electronic states of the free RG atoms. Thus, it is a general trend for weak interacting systems, and hence, it can be useful in determining the position of the electronic states of adsorbates in adsorbate-substrate systems.

Furthermore, we find that $C_{\mathrm{RG}}^{\mathrm{vac}}(\text{on-top}) \approx C_{\mathrm{RG}}^{\mathrm{vac}}(\mathrm{fcc})$ for all systems and XC functionals. However, the same does not hold true for $C_{\mathrm{RG}}^{\mathrm{E_F}}$. The values of $C_{\mathrm{RG}}^{\mathrm{E_F}}$ depend on the work function of the RG/Pd(111) system, which is site dependent, and hence, $C_{\mathrm{RG}}^{\mathrm{E_F}}$ is also a site-dependent function. Using the fact that $|C_{\mathrm{RG}}^{\mathrm{vac}}| = |C_{\mathrm{RG}}^{\mathrm{E_F}}| + \Phi^{\mathrm{RG/Pd(111)}}$ and $C_{\mathrm{RG}}^{\mathrm{vac}}(\text{on-top}) \approx C_{\mathrm{RG}}^{\mathrm{vac}}(\mathrm{fcc})$, we can deduce that $|C_{\mathrm{RG}}^{\mathrm{E_F}}(\text{on-top})| - |C_{\mathrm{RG}}^{\mathrm{E_F}}(\mathrm{fcc})| = \Delta\Phi^{(\mathrm{fcc})} - \Delta\Phi^{(\text{on-top})}$. From Table V, it can be seen that $|C_{\mathrm{RG}}^{\mathrm{E_F}}(\text{on-top})| > |C_{\mathrm{RG}}^{\mathrm{E_F}}(\mathrm{fcc})|$ for all systems and XC functionals [except for He (GGA-PBE and GGA-PW91)]. Thus, we can conclude that $|\Delta\Phi^{(\text{on-top})}| > |\Delta\Phi^{(\mathrm{fcc})}|$ for all systems and

TABLE V. Analysis of the RG local density of states (LDOS) for RG/Pd(111) in the $\sqrt{3}$ structure at the equilibrium geometry. The center of gravity of the RG-LDOS with respect to the Fermi level, $C_{\mathrm{RG}}^{\mathrm{E_F}}$, and vacuum level, $C_{\mathrm{RG}}^{\mathrm{vac}}$, is given. The energy of the highest occupied state of the free He, Ne, Ar, Kr, and Xe atoms is $\varepsilon_{\mathrm{RG}}$ with respect to the vacuum level.

	XC	site	He	Ne	Ar	Kr	Xe
$C_{\mathrm{RG}}^{\mathrm{E_F}}$ (eV)	LDA	on-top	−10.12	−8.21	−5.52	−4.82	−4.34
		fcc	−10.01	−8.16	−5.37	−4.65	−4.18
	GGA-PBE	on-top	−10.54	−8.14	−5.22	−4.33	−3.79
		fcc	−10.55	−8.12	−5.13	−4.24	−3.54
	GGA-PW91	on-top	−10.57	−8.16	−5.22	−4.36	−3.80
		fcc	−10.59	−8.14	−5.12	−4.23	−3.53
$C_{\mathrm{RG}}^{\mathrm{vac}}$ (eV)	LDA	on-top	−15.62	−13.65	−10.51	−9.52	−8.57
		fcc	−15.57	−13.66	−10.49	−9.51	−8.55
	GGA-PBE	on-top	−15.76	−13.34	−10.29	−9.27	−8.26
		fcc	−15.76	−13.33	−10.28	−9.26	−8.25
	GGA-PW91	on-top	−15.86	−13.43	−10.35	−9.31	−8.31
		fcc	−15.86	−13.42	−10.34	−9.31	−8.29
$\varepsilon_{\mathrm{RG}}$ (eV)	LDA		−15.52	−13.55	−10.41	−9.51	−8.63
	GGA-PBE		−15.76	−13.35	−10.30	−9.36	−8.47
	GGA-PW91		−15.87	−13.45	−10.36	−9.41	−8.52

XC functionals [except for He (GGA-PBE and GGA-PW91)], which was, in fact, obtained by our all-electron calculations. As discussed before, a larger value for $\Delta\Phi$ correlates with a stronger interaction with the surface. Therefore, a shift of the LDOS for a particular RG adatom in the fcc site toward the Fermi level indicates a weaker interaction of the RG adatom with the surface.

From the LDOS shown in Fig. 5, it can be seen that there is a clear broadening of the RG-LDOS, which occurs due to the interaction between RG atoms and Pd(111), as well as due to the RG adatom-adatom interactions. A larger interaction between the RG atom and Pd(111) implies a larger broadening of the RG-LDOS. For example, the largest (smallest) broadening occurs for Xe (He) adatoms, which correlates with the magnitude of the electron density differences, work function changes (induced dipole moment), and adsorption energies. There is a clear depopulation of the Ne, Ar, Kr, and Xe p states, i.e., the tails of the p states (mainly p_z symmetry) extend above the Fermi level and become depopulated. Furthermore, there is a partial occupation of the previously unoccupied RG s and d states, which extend below the Fermi level and become occupied. The magnitude of the occupation increases from He to Xe, i.e., larger for RG atoms that are strongly bound to the Pd(111) surface.

IV. ROLE OF THE ELECTRONIC POLARIZABILITIES OF THE RARE-GAS ATOMS IN THE ADSORPTION PROPERTIES OF RARE-GAS/Pd(111)

To obtain a better understanding of the nature of the interaction between RG atoms and Pd(111), we investigate the correlation between the magnitude of the adsorption properties, namely, the adsorption energy and induced dipole moment (work function change) and the electronic polarizability of the free RG atoms. The electronic polarizabilities of the He, Ne, Ar, Kr, and Xe atoms, α^{RG}, are 0.201×10^{-24}, 0.390×10^{-24}, 1.62×10^{-24}, 2.46×10^{-24}, and 3.99×10^{-24} cm^3, respectively.[37] The polarizability ratios with respect to the Xe atoms $\left(\frac{\alpha^{\mathrm{Xe}}}{\alpha^{\mathrm{RG}}}\right)$ are 19.85, 10.23, 2.46, 1.62, and 1.00 for He, Ne, Ar, Kr, and Xe, respectively, while the LDA adsorption energy ratios with respect to the Xe adatoms $\left(\frac{E_{\mathrm{ad}}^{\mathrm{Xe}}}{E_{\mathrm{ad}}^{\mathrm{RG}}}\right)$ are 16.31, 6.61, 2.73, 1.93, and 1.00, for He, Ne, Ar, Kr, and Xe atoms, respectively. The good agreement between the polarizabilities and adsorption energy ratios suggests a correlation between the adsorption properties of RG/Pd(111) and electronic polarizability of the free RG atoms.

We calculate the adsorption energies and induced dipole moments of RG adatoms on Pd(111) using the DFT results and the electronic polarizabilities of the free RG atoms. For example,

$$E_{\mathrm{ad},\alpha}^{\mathrm{RG}} = \frac{E_{\mathrm{ad}}^{\mathrm{Xe}}}{\alpha^{\mathrm{Xe}}}\alpha^{\mathrm{RG}}, \tag{6}$$

where $E_{\mathrm{ad}}^{\mathrm{Xe}}$ is the calculated DFT adsorption energy and α^{RG} is the electronic polarizability of the free RG atom. Thus, $E_{\mathrm{ad},\alpha}^{\mathrm{RG}}$ can be calculated using different RG atoms as reference, e.g., the DFT adsorption energy of Ar, $E_{\mathrm{ad}}^{\mathrm{Ar}}$, along with α^{RG} and α^{Ar} can be used to calculate $E_{\mathrm{ad},\alpha}^{\mathrm{RG}}$ for He, Ne, Ar, Kr, and Xe adatoms [just as Eq. (6) using Xe as reference]. The same procedure applies for estimating the induced dipole moments $\mu_{\alpha}^{\mathrm{RG}}$ for all RG adatoms. The results for $E_{\mathrm{ad},\alpha}^{\mathrm{RG}}$ and $\mu_{\alpha}^{\mathrm{RG}}$ using all the calculated LDA, GGA-PBE, and GGA-PW91 results as reference are plotted in Fig. 6.

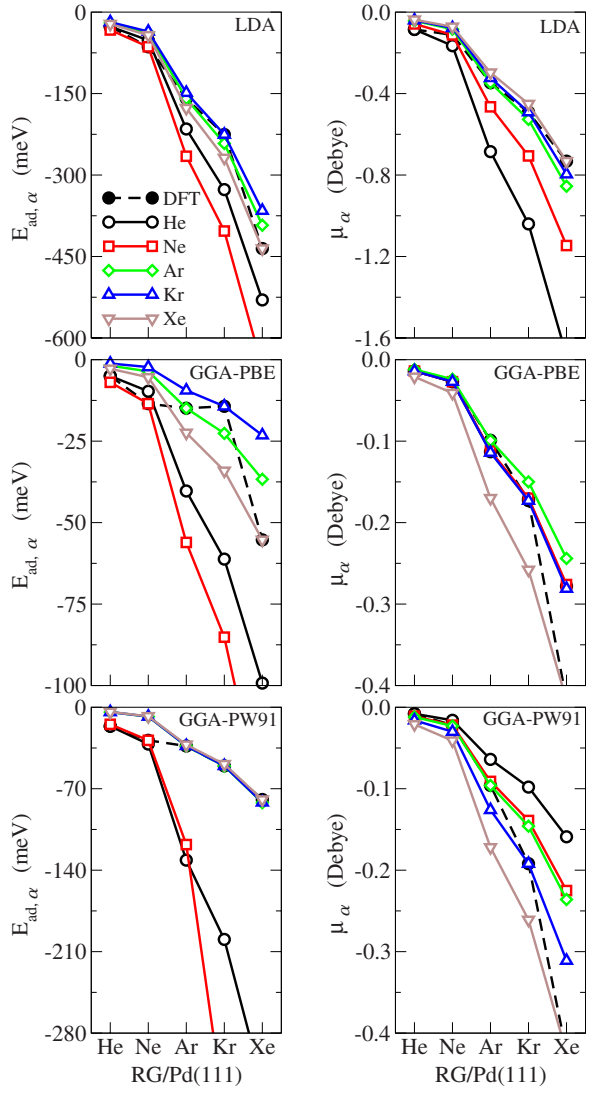

FIG. 6. (Color online) Estimated adsorption energy $E_{\mathrm{ad},\alpha}^{\mathrm{RG}}$ and induced dipole moment $\mu_{\alpha}^{\mathrm{RG}}$ of RG adatoms in the on-top sites on Pd(111) in the $\sqrt{3}$ structure using the electronic polarizability ratio of the free RG atoms. Dashed lines with filled circles indicate the calculated DFT adsorption energies and induced dipole moments. The open circle, square, diamond, triangle-up, and triangle-down symbols indicate results for $E_{\mathrm{ad},\alpha}^{\mathrm{RG}}$ and $\mu_{\alpha}^{\mathrm{RG}}$ calculated using the electronic polarizability ratios of the free RG atoms and the DFT results for $E_{\mathrm{ad}}^{\mathrm{RG}}$ and μ^{RG} of the He, Ne, Ar, Kr, and Xe adatoms, respectively.

We find that using the LDA adsorption energies of Ar, Kr, and Xe as reference, combined with α^{RG}, yield results for the estimated adsorption energy ($E_{\mathrm{ad},\alpha}^{\mathrm{RG}}$) in very good agreement with the directly calculated LDA values for Ar, Kr, and Xe adatoms; however, it yields slightly smaller adsorption energies for He and Ne compared with the LDA values. Using the DFT adsorption energy of He or Ne as reference, it can be seen that the estimated adsorption energies for Ar, Kr, and Xe are notably overestimated, e.g., using Ne as reference $E_{\mathrm{ad},\alpha}^{\mathrm{Xe}}$=−653.7 meV (lying off the plot) compared with the DFT-LDA value of −435.4 meV. This may indicate a larger relative overestimation of the adsorption energy for He and Ne, which is also indicated by the (estimated) experimental results shown in Fig. 2. With regard to the surface dipole moment, shown in Fig. 6, a similar trend is obtained.

For the results obtained using the GGA-PBE and GGA-PW91 functionals, a similar trend to that described above is found. Namely, using the Ar, Kr, and Xe atoms as reference to estimate the adsorption energies of the other RG atoms, together with the polarizabilities of the free RG atoms, the resulting adsorption energies are rather close to the actual DFT-GGA values but using Ne and He as reference, all adsorption energies are significantly overestimated.

For the induced dipole moments, using the GGA-PBE values of all except Xe as reference yields estimated values of all RG atoms (except for Xe) in good agreement with the direct DFT results. The values estimated for the dipole moment of Xe are notably underestimated. Using Xe as reference overestimates somewhat the induced dipole moments of the other RG/Pd(111) systems. For the GGA-PW91, a similar behavior is found, although there is more spread in all the values.

In general, our analysis provides indication of a correlation between the adsorption energies and the electronic polarizabilities of the RG adatoms, which is particularly striking when using Ar, Kr, and Xe as reference.

V. INTERACTION MECHANISM BETWEEN RARE-GAS ATOMS AND THE Pd(111) SURFACE

All the DFT-LDA, -GGA-PBE, and -GGA-PW91 calculations show that the interaction between RG atoms and Pd(111) induces a polarization of the RG atoms as they adsorb on the Pd(111) surface. In Ref. 26, we showed that this polarization systematically increases as the RG atom approaches the surface. Our analysis of the electron density redistribution of the RG adatoms and of the induced dipole moment (work function change) shows that the polarization of the RG adatoms increases from He to Xe. The trend in the magnitude of the polarization of the RG adatoms is determined largely by the magnitude of the electronic polarizability of the free RG atoms, as revealed by the correlation of the adsorption energy and induced dipole moment. Furthermore, there is a strong polarization of the Pd atoms in the topmost surface layer upon the adsorption of RG atoms, which is weaker for He and larger for Xe adatoms.

In our earlier publications,[24,26] it was shown that the electronic character of the clean Pd(111) surface at the on-top region is donorlike and in the fcc site region it is acceptorlike. Hence, it plays an important role in the screening of the perturbation induced by the RG adatoms, as well as in the site dependence of the Pauli repulsion. For example, at close distances where wave functions start to overlap and Pauli repulsion sets in between the closed shell RG atom and the electrons at the Fermi energy, it was found that the substrate can reduce this repulsion more efficiently at the on-top site by transferring electrons from the on-top site region to the hollow site region, and hence, RG adatoms can get closer to the surface at the on-top site at the equilibrium geometry.

Considering the magnitude of the induced dipole moments and equilibrium RG-Pd(111) distances, the LDA func-

tional gives a larger polarization and a weaker Pauli repulsion for RG adatoms in the on-top sites. Thus, it results in greater attractive and weaker repulsive interactions between the RG atoms and the Pd(111) surface. Hence, these mechanisms favor the on-top site preference for RG adatoms on Pd(111), which was obtained by the LDA for all the RG systems. We note that the on-top site preference is favorable by less than 2 and 4 meV for Ne and He adatoms, respectively, which is close to the limit of the accuracy of the present calculations.

The magnitude of the induced dipole moment and the equilibrium RG-Pd(111) distances are larger and smaller, respectively, for Xe, Kr, and Ar adatoms in the on-top site, which favors the on-top site preference. However, GGA calculations yielded the on-top site preference for Xe and Kr adatoms, while the fcc site was preferred for Ar. As pointed out in the previous section, the fcc site preference for Ar adatoms Pd(111) should be taken with caution due to the inconsistency between the trends in the induced dipole moment, equilibrium distances, and the relative adsorption energy, which could be related to the limits of accuracy of the present calculations. For Ne adatoms, both GGA functionals yield almost the same equilibrium distance for the on-top and fcc sites, but a slightly greater induced dipole moment for the on-top site. Hence, there is no strong indication for the adsorption site preference based on the polarization and site-dependent Pauli repulsion for Ne adatoms, which is consistent with the total energy calculations, i.e., the fcc site is favorable by less than 1 meV so both sites are essentially degenerate within the accuracy of the present calculations. For He, both GGA functionals yield a larger induced dipole moment and smaller equilibrium RG-Pd(111) distances for He adatoms in the fcc site, which would seem to favor adsorption of He atoms in the fcc site; however, the total energy GGA calculations find the on-top site favorable, albeit by very small values of 2.5 and 1.4 meV.

In summary, our results indicate that polarization effects of the RG adatoms and Pd atoms in the topmost surface layer and the site dependence of the Pauli repulsion determine the interaction between RG atoms and the Pd(111) surface. However, a complete trend for the RG on-top site preference on Pd(111) is not obtained due to the discrepancies between LDA and GGA (PBE and PW91) functionals for Ar and Ne.

VI. PERFORMANCE OF LDA, GGA-PBE, AND GGA-PW91 IN THE STUDY OF RARE GAS/Pd(111)

The existence of well established experimental data is an important prerequisite for the study of the performance of XC functionals in DFT. Unfortunately, for the present systems, there are available experimental results only for Xe/Pd(111), so it is difficult to evaluate the performance of the LDA, GGA-PBE, and GGA-PW91 functionals. Thus, in the present discussion, we will provide only a qualitative discussion of the performance.

At far distances from the solid surface in which there is no overlap of the RG and substrate orbitals, the attractive interaction potential is determined by the well known van der Waals interaction (dispersion forces), which is not correctly described by DFT-LDA/GGA. For example, the asymptotic limit of the potential energy at large RG-surface separation is $1/Z^3$ (Ref. 62); however, DFT-LDA/GGA leads to an asymptotic limit as $1/Z^p$ with $p>3$. At closer distances to the equilibrium RG-surface geometry, the substrate induces a polarization of the RG adatoms and a direct interaction between the RG and substrate orbitals sets in. In this regime, it is expected that DFT-LDA/GGA can provide at least a qualitative description of the interaction between RG atoms and the solid surface, which has been shown to be true for several systems, e.g., Xe/metal,[23–26] [He,Ne]/Ru(0001),[40] and Xe adsorption on the graphite (0001) surface.[30,31]

The LDA yields work function changes larger than GGA (PBE and PW91), which is a consequence of the smaller equilibrium RG-Pd(111) distances obtained by LDA compared to the GGA results. In particular, the absolute value of the work function change increases almost linearly as the RG adatoms approach the surface,[24–26] and hence, a smaller equilibrium RG-Pd(111) distance as obtained by the LDA functional implies a larger work function change. LDA and GGA calculations performed for RG adatoms at the same height above the surface yield work function changes with similar value.[24,26] For Xe/Pd(111), the LDA work function change (−1.435 eV) is significantly larger than the experimental result (−0.85 eV); however, the GGA-PBE and GGA-PW91 work function changes, −0.778 and −0.791 eV, respectively, are in reasonable agreement with the experimental value. This is nevertheless fortuitous and due to the overestimation of the equilibrium distance by the GGA functionals. Thus, it is not an indication of a superior description by the GGA functionals. A quantitative description of the work function change, as well as the electron density differences, depends critically on the correct description of the equilibrium distances.

For Xe/Pd(111), the LDA adsorption energy (−435 meV) is in better agreement with the experimental results (−320±10 and −360 meV) than the GGA (PBE and PW91) results (−55 and −79 meV). Furthermore, using our LDA results, we obtained $E_{ad}^{Xe}/E_{ad}^{Kr}=1.93$ and $E_{ad}^{Xe}/E_{ad}^{Ar}=2.73$, which are in good agreement with experimental values (2 and 3). The GGA results yielded significantly smaller ratios. The GGA-PBE adsorption energy is almost constant for Ne, Ar, and Kr adatoms on Pd(111), which is an unexpected result. Therefore, at least for the adsorption energy of the Xe, Kr, and Ar adatoms, the LDA results and trends are superior to those of the GGA.

VII. SUMMARY

In this work, we reported a systematic study of the interaction of RG atoms with the Pd(111) surface in the $\sqrt{3}$ structure employing DFT using the LDA, GGA-PBE, and GGA-PW91 functionals. All calculations were performed with the all-electron FP-LAPW method, which is one of the most accurate methods to solve the Kohn-Sham equations.

The LDA, GGA-PBE, and GGA-PW91 results indicate that polarization effects of the RG adatoms and Pd atoms in the topmost surface layer and the site dependence of the Pauli repulsion determine the interaction between the RG

atoms and the Pd(111) surface. Analysis of the induced dipole moment and adsorption energy indicates that the trends in the magnitude scale approximately with the electronic polarizability of the free RG atoms.

The LDA, GGA-PBE, and GGA-PW91 functionals yield very similar trends for the electron density redistribution, work function changes (induced dipole moments), and center of gravity of the RG-LDOS. The results differ only in the magnitude of the values due to the underestimation and overestimation of the equilibrium RG-Pd(111) distances by the LDA and GGA (PBE and PW91), respectively. For example, the LDA (GGA-PBE and GGA-PW91) yields larger (smaller) electron density redistribution and work function changes due to the smaller (larger) RG-Pd(111) separation.

The LDA, GGA-PBE, and GGA-PW91 functionals show important differences for properties such as the RG adsorption site preference on Pd(111). For example, LDA favors the on-top site for all RG adatoms on Pd(111); however, GGAs (PBE and PW91) yield the on-top site preference for Xe, Kr, and He adatoms, while Ne and Ar adatoms preferentially bind to the fcc sites. We note, however, here the energy difference between on-top and fcc sites for Ne and He (LDA), and Ar, Ne, and He (GGA-PBE and GGA-PW91) are very small (<5 meV).

Thus, only the LDA functional yields a general trend for the RG on-top site preference, which seems to be consistent with experimental observations for RG adatoms on metal surfaces,[15–21,33,34] which is in contrast with GGA (PBE and PW91) calculations for Ar and Ne adatoms on Pd(111) which predicts an fcc site preference. The present results indicate that a theoretical approach beyond the DFT-LDA/GGA framework (e.g., van der Waals density-functional theory[63]) is required in order to solve these differences between local and semilocal XC functionals, as well as to provide deeper insights. In addition, experimental results for RG (He, Ne, Ar, Kr) on Pd(111) would be most valuable.

ACKNOWLEDGMENTS

We thank Matthias Scheffler for fruitful discussions and the Fritz-Haber Institute of the Max-Planck Society and the Australian Center for Advanced Computing and Communications for the computational resources.

*Present address: National Renewable Energy Laboratory, 1617 Cole Boulevard, Golden, CO 80401, USA; juarez_dasilva@nrel.gov

†stampfl@physics.usyd.edu.au

[1] L. W. Bruch, M. W. Cole, and E. Zaremba, *Physical Adsorption: Forces and Phenomena* (Oxford Science, Oxford, 1997).

[2] K. Wandelt and J. E. Hulse, J. Chem. Phys. **80**, 1340 (1984).

[3] G. Vidali, G. Ihm, H.-Y. Kim, and M. W. Cole, Surf. Sci. Rep. **12**, 133 (1991).

[4] P. Zeppenfeld, *Physics of Covered Solid Surfaces*, Landolt-Börnstein, New Series, Group III, Vol. 42, Pt. A (Springer-Verlag, Berlin, 2001), p. 67.

[5] J. F. Zhu, H. Ellmer, H. Malissa, T. Brandstetter, D. Semrad, and P. Zeppenfeld, Phys. Rev. B **68**, 045406 (2003).

[6] E. Hulpke, *Helium Atom Scattering from Surfaces* (Springer, Heidelberg, 1992).

[7] L. D. de Menorval, J. P. Fraissard, and T. Ito, J. Chem. Soc., Faraday Trans. 1 **78**, 403 (1982).

[8] A. Bifone, T. Pietrass, J. Kritzenberger, A. Pines, and B. F. Chmelka, Phys. Rev. Lett. **74**, 3277 (1995).

[9] K. Wandelt, J. Vac. Sci. Technol. A **2**, 802 (1984).

[10] G. A. Hishmeh, L. Cartz, F. Desage, C. Templier, J. C. Desoyer, and R. C. Birtcher, J. Mater. Res. **9**, 3095 (1994).

[11] K. Mitsuishi, M. Kawasaki, M. Takeguchi, and K. Furuya, Phys. Rev. Lett. **82**, 3082 (1999).

[12] M. Gsell, P. Jakob, and D. Menzel, Science **280**, 717 (1998).

[13] P. Jakob, M. Gsell, and D. Menzel, J. Chem. Phys. **114**, 10075 (2001).

[14] B. N. J. Persson, Surf. Sci. Rep. **33**, 83 (1999).

[15] B. Narloch and D. Menzel, Chem. Phys. Lett. **290**, 163 (1997).

[16] B. Narloch and D. Menzel, Surf. Sci. **412**, 562 (1998).

[17] Th. Seyller, M. Caragiu, R. D. Diehl, P. Kaukasoina, and M. Lindroos, Chem. Phys. Lett. **291**, 567 (1998).

[18] R. D. Diehl, T. Seyller, M. Caragiu, G. S. Leatherman, N. Ferralis, K. Pussi, P. Kaukasoina, and M. Lindroos, J. Phys.: Condens. Matter **16**, S2839 (2004).

[19] Th. Seyller, M. Caragiu, R. D. Diehl, P. Kaukasoina, and M. Lindroos, Phys. Rev. B **60**, 11084 (1999).

[20] M. Caragiu, Th. Seyller, and R. D. Diehl, Phys. Rev. B **66**, 195411 (2002).

[21] M. Caragiu, Th. Seyller, and R. D. Diehl, Surf. Sci. **539**, 165 (2003).

[22] J. E. Müller, Phys. Rev. Lett. **65**, 3021 (1990).

[23] A. E. Betancourt and D. M. Bird, J. Phys.: Condens. Matter **12**, 7077 (2000).

[24] J. L. F. Da Silva, Ph.D. thesis, Technical University of Berlin, 2002, http://edocs.tu-berlin.de/diss/2002/dasilva_juarez.htm, http://www.fhi-berlin.mpg.de/th/pub02.html

[25] J. L. F. Da Silva, C. Stampfl, and M. Scheffler, Phys. Rev. Lett. **90**, 066104 (2003).

[26] J. L. F. Da Silva, C. Stampfl, and M. Scheffler, Phys. Rev. B **72**, 075424 (2005).

[27] P. S. Bagus, V. Staemmler, and C. Wöll, Phys. Rev. Lett. **89**, 096104 (2002).

[28] S. Clarke, G. Bihlmayer, and S. Blügel, Phys. Rev. B **63**, 085416 (2001).

[29] K. Pussi, J. Smerdon, N. Ferralis, M. Lindroos, R. MacGrath, and R. D. Diehl, Surf. Sci. **548**, 157 (2004).

[30] X.-R. Chen, X.-L. Zhou, J. Zhu, and Q.-Q. Gou, Phys. Lett. A **315**, 403 (2003).

[31] J. L. F. Da Silva and C. Stampfl, Phys. Rev. B **76**, 085301 (2007).

[32] S. Wilke, M. H. Cohen, and M. Scheffler, Phys. Rev. Lett. **77**, 1560 (1996).

[33] Th. Seyller, M. Caragiu, and R. D. Diehl, Surf. Sci. **454**, 55 (2000).

[34] M. Caragiu, G. S. Letherman, Th. Seyller, and R. D. Diehl, Surf.

Sci. **475**, 89 (2001).
[35] Y. C. Chen, J. E. Cunningham, and C. P. Flynn, Phys. Rev. B **30**, 7317 (1984).
[36] C. Hückstädt, S. Schmidt, S. Hüfner, F. Forster, F. Reinert, and M. Springborg, Phys. Rev. B **73**, 075409 (2006).
[37] C. Kittel, *Introduction to Solid State Physics*, 7th ed. (Wiley, New York, 1996).
[38] P. Hohenberg and W. Kohn, Phys. Rev. **136**, B864 (1964).
[39] W. Kohn and L. J. Sham, Phys. Rev. **140**, A1133 (1965).
[40] M. Petersen, S. Wilke, P. Ruggerone, B. Kohler, and M. Scheffler, Phys. Rev. Lett. **76**, 995 (1996).
[41] J. P. Perdew, J. A. Chevary, S. H. Vosko, K. A. Jackson, M. R. Pederson, D. J. Singh, and C. Fiolhais, Phys. Rev. B **46**, 6671 (1992).
[42] J. P. Perdew and Y. Wang, Phys. Rev. B **45**, 13244 (1992).
[43] J. P. Perdew, K. Burke, and M. Ernzerhof, Phys. Rev. Lett. **77**, 3865 (1996).
[44] D. C. Patton and M. R. Pederson, Phys. Rev. A **56**, R2495 (1997).
[45] D. J. Singh, *Plane Waves, Pseudopotentials and the LAPW Method* (Kluwer Academic, Boston, 1994).
[46] P. Blaha, K. Schwarz, P. Sorantin, and S. B. Trickey, Comput. Phys. Commun. **59**, 399 (1990).
[47] A. Khein, D. J. Singh, and C. J. Umrigar, Phys. Rev. B **51**, 4105 (1995).
[48] A. Zupan, P. Blaha, K. Schwarz, and J. P. Perdew, Phys. Rev. B **58**, 11266 (1998).
[49] M. Fuchs, J. L. F. Da Silva, C. Stampfl, J. Neugebauer, and M. Scheffler, Phys. Rev. B **65**, 245212 (2002).
[50] H. J. Monkhorst and J. D. Pack, Phys. Rev. B **13**, 5188 (1976).
[51] M. G. Gillan, J. Phys.: Condens. Matter **1**, 689 (1989).
[52] J. L. F. Da Silva, C. Stampfl, and M. Scheffler, Surf. Sci. **600**, 703 (2006).
[53] F. D. Murnaghan, Proc. Natl. Acad. Sci. U.S.A. **50**, 697 (1944).
[54] K. Kern, R. David, P. Zeppenfeld, and G. Comsa, Surf. Sci. **195**, 353 (1988).
[55] F. Brunet, R. Schaub, S. Fédrigo, R. Monot, J. Buttet, and W. Harbich, Surf. Sci. **512**, 201 (2002).
[56] K. Wandelt and B. Gumhalter, Surf. Sci. **140**, 355 (1984).
[57] J. F. Olgivie and F. Y. H. Wang, J. Mol. Struct. **273**, 277 (1992).
[58] J. F. Olgivie and F. Y. H. Wang, J. Mol. Struct. **291**, 313 (1993).
[59] T. Fauster and W. Steinman, *Electromagnetic Waves: Recent Developments in Research* (Elsevier, Amsterdam, 1995).
[60] R. Gomer, Acc. Chem. Res. **29**, 284 (1996).
[61] L. D. Schmidt and R. Gomer, J. Chem. Phys. **45**, 1605 (1966).
[62] E. Zaremba and W. Kohn, Phys. Rev. B **13**, 2270 (1976).
[63] S. D. Chakarova-Käck, E. Schröder, B. I. Lundqvist, and D. C. Langreth, Phys. Rev. Lett. **96**, 146107 (2006).